www.czasopisma.pan.pl PAN POLSKA AKADEMIA NAUK www.journals.pan.pl

PAN ARCHIVES OF ACOUSTICS
Vol. **45**, No. 2, pp. 221–231 (2020)
DOI: 10.24425/aoa.2020.133143

Research Paper

Comparison of Acoustic Emission Data Acquired During Tensile Deformation of Maraging Steel M250 Welded Specimens

Gowri Shankar WURITI(1)*, Somnath CHATTOPADHYAYA(1), Grzegorz KROLCZYK(2)

(1) *Department of Mechanical Engineering, Indian Institute of Technology (ISM)*
Dhanbad, India
*Corresponding Author e-mail: wuritigshankar@gmail.com

(2) *Department of Manufacturing Engineering and Automation Products*
Opole University of Technology
Opole, Poland

(*received October 3, 2019; accepted January 17, 2020*)

Safety and reliability are primary concerns in launch vehicle performance due to the involved costs and risk. Pressure vessels are one of the significant subsystems of launch vehicles. In order to have minimal weight, high strength material *viz.* maraging steel M250 grade is used in realizing the pressure vessel casing hardware. Despite the best efforts in design methodology, quality evaluation in production and effective structural integrity assessment is still a farfetched goal. The evolution of such a system requires, first, identification of an appropriate technique and next its adoption to meet the challenges posed by advanced materials like maraging steels. In fact, a quick survey of the available Non-Destructive Evaluation (NDE) techniques suggests Acoustic Emission (AE) as an effective structural integrity assessment tool capable of identifying any impending failure or degradation at an earlier stage. Experience shows that the longitudinal welds in the pressure vessels are quite vulnerable to failure due to the fact that they experience the maximum stress (i.e. hoop stress). Loading welded tensile samples are quite synonymous to the hoop stress experienced by longitudinal welds. An attempt is made to compare the Acoustic Emission data acquired during tensile deformation of maraging steel welded specimens. A total of 16 welded specimen's with known defects were studied for their tensile behaviour is in connection with Acoustic Emission data. The lowest failure load was 70.5 kN and the highest being 84.8 kN. AE activity graphs viz. cumulative AE activity, hit rate, energy rate, count rate, AE amplitude history, AE count history, AE energy history, amplitude-count correlation and hit amplitude distribution have been investigated and salient features with respect to the data have been critically studied and relevant correlations are arrived at.

Keywords: maraging steel M250 grade; Acoustic Emission (AE); stress strain.

1. Introduction

The rocket motors are one of the significant subsystems for the spacecraft vehicles and rockets. Ultra high strength steels like maraging steel M250 are being extensively used in order to attain extended range and increased pay load capabilities. Such high strength steels are relatively brittle and fracture prone. Hence, fracture control becomes the primary focal point in the quality assurance methodology. Fabrication processes inflict certain defects which are mostly unavoidable. Various NDT methods are used to diagnose and characterize such defects. In spite of the best efforts to screen the vessels for presence of defects through radiography method, certain faint radiographic indications, which are otherwise acceptable as per established standards and design point of view are observed. These types of micro defects are generally sub-critical and do not cause any failure. However, upon nucleation of micro voids and defects, results in the dynamic growth of the defect due to the application of mechanical load. The growth of these micro defects transform into critical or super-critical size defects that leads to catastrophic failure. During proof pressure testing, there is no indicator for detecting degradation of structural integrity of these pressure vessels due to the growth of

the defects. In spite of extensive strain gauging during proof pressure test, the exact information about crack growth process in the vicinity of the welded regions may be illusive. Acoustic Emission technique is a standardized technique and can assess almost the entire system being tested with few sensors/transducers (Hsu, Hardy, 1978). The AE technique identifies defects and discontinuities in terms of AE parameters *viz.* amplitude, counts, duration, energy, etc. Most of these emission sources can be distinguished by their acoustic emission signature (Cross *et al.*, 1972; Wuriti *et al.*, 2019). The severity can be analysed quantitatively based on high energy emissions which are subsequently characterized by high amplitude as well as long duration events (Hay *et al.*, 1984). It has been reported that Acoustic Emission data could be effectively used to evaluate the residual strength in terms of burst pressure, etc. of pressure vessel casings (Hill *et al.*, 1992; Chelladurai *et al.*, 1996).

The initial step is to understand the characteristic behaviour of maraging steel during the tensile deformation and the corresponding AE signals. Some efforts have been put in to comprehend AE Signal characteristics of stress corrosion cracks (SCC) in SS304 material. Based on AE waveforms, SCC stages were identified (Hwang *et al.*, 2015). In another study the dependence of AE signal amplitude on crack increment area has been reported (Skalskyi *et al.*, 2018). Another study reported that absolute energy of AE was more suitable for fatigue life prediction (Yu *et al.*, 2011). Acoustic emission count rate has been investigated during tensile loading of magnesium AZ alloys and found to have a direct implication on the grain size (Bohlen *et al.*, 2004). In a study, AE performance of maraging steel specimens with inserted surface cracks of different sizes has been studied. The studies have indicated the possibility of failure prediction prior to rupture. The AE data presented in a conducive form enabling real time evaluation of the material (Chelladurai *et al.*, 1995). In another study, it has been shown that statistical parameters that are derived from AE amplitude distribution have been used for prediction of failure loads (Wuriti *et al.*, 2019).

Such studies would be a crucial step in using acoustic emission testing as a tool for structural integrity evaluation of maraging steel casing pressure vessels. In this work an effort is put forward towards quantitative assessment of the failure in maraging steel specimens that undergo tensile deformation. This shall gradually lead towards predicting structural integrity assessment of pressure vessel casings in an effective mean.

2. AE monitoring and data acquisition

The on-line whole field AE system, Make Physical Acoustics® with AEWin® software is a fully digital, multi-channel, computerized system that performs AE waveform and signal measurement and stores that displays and analyses the resulting data.

Highly sensitive piezo-electric transducers, Physical Acoustics® Make R15I, 150 kHz, Resonant type are used to acquire acoustic emissions from the maraging steel test specimens. Its frequency response is characterized by a peak at 150 kHz where it exhibits a resonance. It is suitable for almost all Acoustic Emission application and especially suited for integrity inspection of metallic structures. The amplitude-frequency characteristic is shown in Fig. 2.

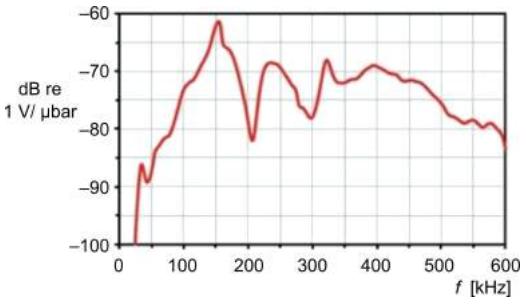

Fig. 2. Amplitude-frequency characteristic of AE sensor.

The voltage output signal from the AE transducer, which is of the order of few millivolts, is fed to a preamplifier with a gain of 40 dB (× 100). The preamplifier, Physical Acoustics® Make, type 2/4/6 at 40 dB also houses a plug in filter, in this case with a band pass

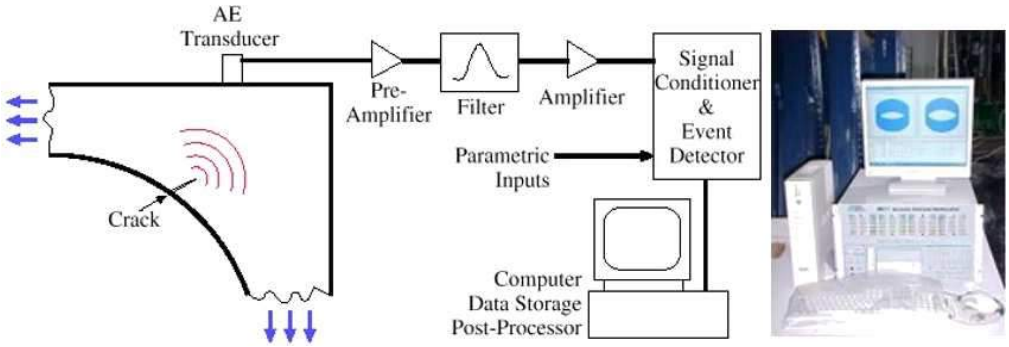

Fig. 1. Schematic block diagram of AE system.

of 100 kHz – 1.2 MHz. This range is chosen to avoid to the possible extent the noise generated by sources such as high-pressure oil flow in the actuator assembly, and the hydraulic grips, frictional and vibration noises generated in the fixture accessories, etc. Experience has shown that most of these noises fall in the lower frequency range with a maximum up to 100 kHz. Further, a wide band of signal above 100 kHz is desirable for extracting a wealth of information about the sources and the phenomenon hidden in the AE signal. Amplified and filtered output from the preamplifier is of the order of hundreds of millivolts to a few volts. The amplified input is then fed into the Data acquisition Setup. In order to avoid background noises, a threshold of 40 dB is applied. The general electrical noises in the setup amount to almost 10 mV in a 40 dB (i.e. 100 times to the reference value) pre-amplified circuit. Hence, any signal crossing this threshold is only acquired and signals crossing this reference gate are only considered for ring-down counts.

3. Experimental evaluation

A total of 16 standard tensile test specimens as per ASTM E8 standard have been subjected to tensile deformation. Typical specimen drawing is given in Fig. 3. Due to higher failure load, serrations are provided in the grip region for improved gripping and thereby arresting the slip of the specimen from specimen holding grips.

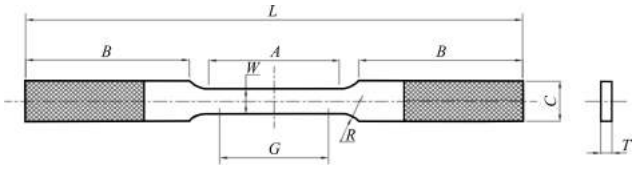

Nomenclature	Specification [mm]
L	200
G	$50^{\pm 0.1}$
W	$12.5^{\pm 0.2}$
B	50
C	20
A	57
R	12.5
T	$5.2^{+0.2}$

Fig. 3. Specimen details.

The specimens are screened by Radiographic and ultrasonic inspections to understand the inherent defects. A 300 kN closed loop, servo-hydraulic dynamic system is used for tensile loading. As per standards 10% of maximum load in 2 minutes, a loading rate of 2.5 kN/min was followed. The specimen as held in the grips of the tensile testing machine with sensors mounted on it is shown in Fig. 4.

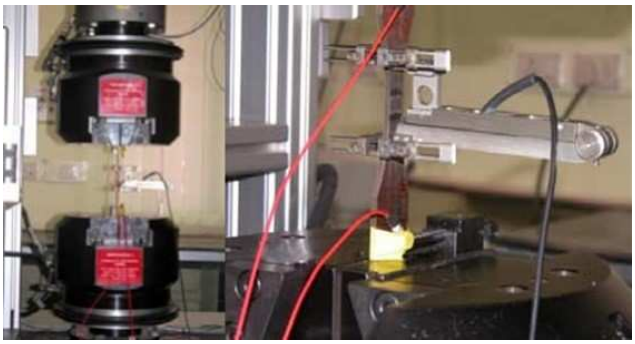

Fig. 4. Specimen loaded onto UTM and sensor placement.

4. Test results and discussions

The AE response monitored is due to the dynamic activity at the weldments, either due to natural defects like pores, inter-granular activity, defect edge, extension and formation of stretch zone and finally followed by unstable rapid fracture. During the initial phase of loading and at least until 50% of the failure loading there is almost very scarce AE activity.

This is almost the same trend in all the specimens irrespective of whether they have a notch/defect or not. Anyhow, for notched specimens, it could be seen that these scarce activities are associated to the location of the notch. Yielding/plastic deformation information could be recorded by comparing the Acoustic Emission activity with actual straining of material (Akbari *et al.*, 2010). Useful information about the behaviour of the specimen could be collected with correlating with AE attributes like amplitude, counts, energy rise time, duration, etc. (Chelladurai *et al.*, 1999). Moreover, AE rate graphs like hit rate, energy rate can be used as better predictors to indicate failure of material (Chelladurai *et al.*, 1995). The amplitude-hit distribution plots are very useful in statistical analysis of the AE data.

Parts of the following drawings are related to following specimens:

a) with inherent micro defects,
b) with defect free weld,
c) with weld defect,
d) with HAZ failure.

4.1. Cumulative AE activity

Cumulative AE activity with respect to stress strain graph is given in Figs 5a to 5d. A sudden change in the slope of the AE activity plot is an indication of onset of damage. Moreover, when such plots are studied in conjunction with stress-strain or load plots, more information could be derived. Figures 5a to 5d represent cumulative AE activity *vs* strain interposed over stress-strain graph. From these graphs, it could be seen that the highest activity has been recorded with the

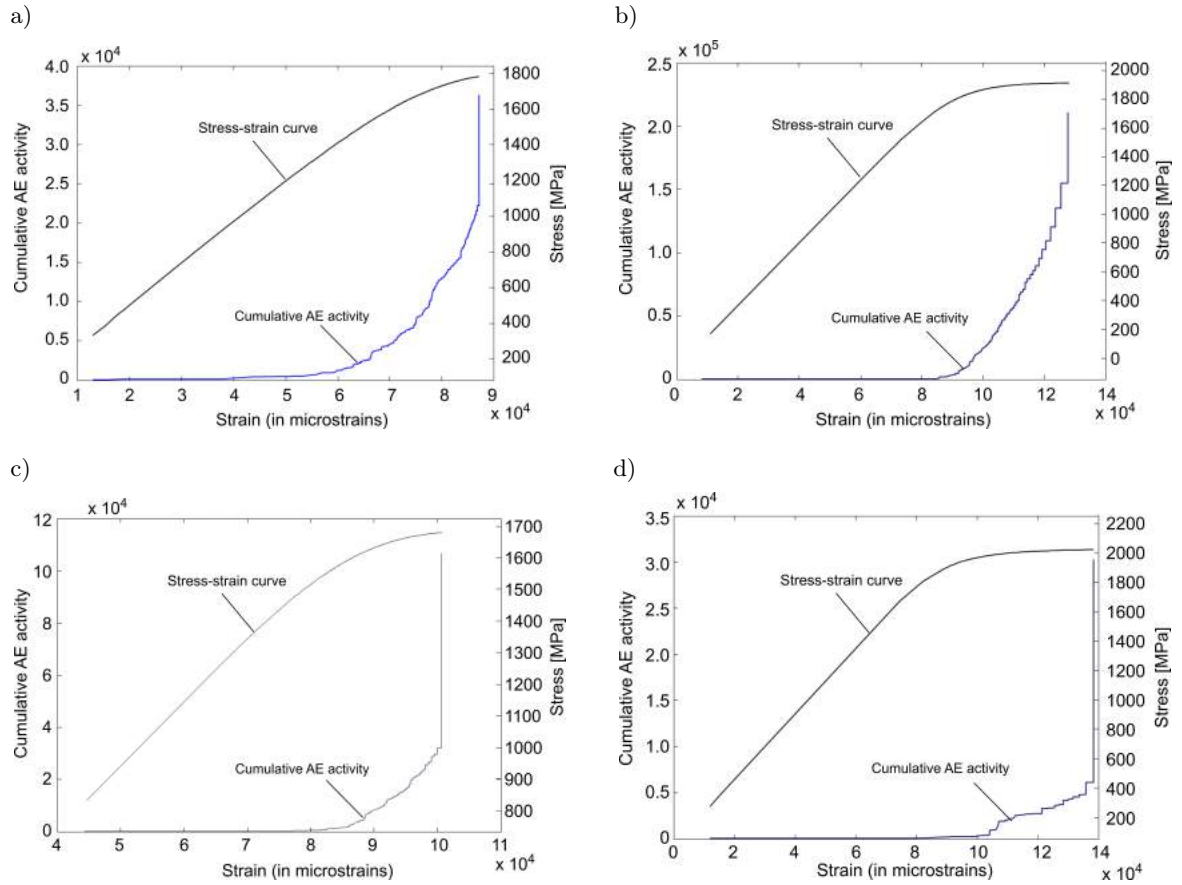

Fig. 5. Cumulative AE activity and stress-strain comparative plot: a) with inherent micro defects, b) with defect free weld, c) with weld defect, d) with HAZ failure.

specimen having a no defect character (Fig. 5b – defect free weld) and the lowest being the one which failed in the heat affected zone (Fig. 5d – HAZ). It could also be seen that a sudden spurt of activity sets in once the linearity of the stress-strain graph changes. Hence, it could be approximately seen that this increase in activity is an indicative of the start of yield in a material (Subba Rao *et al.*, 1996). A rapid change in the slope of the cumulative activity graph is a vivid indicator of onset of failure.

4.2. AE hit rate

Figure 6 represents AE hit rate *vs* strain interposed over stress-strain graph. From these graphs, it could be seen that the hit rate graphs have followed a similar trend as the cumulative graphs present above. Again it could be observed that the highest hit rate has been recorded with the specimen having no defect (Fig. 6b – defect free weld) and the lowest being the one which failed in the heat affected zone (Fig. 6d – HAZ). Moreover, when closely observed, it could be seen that the onset of around 2 hits per second is a clear indicator of change of linearity in the stress-strain curve and is also an effective indicator of impending failure.

4.3. AE energy rate

Figure 7 represents AE energy rate *vs* strain interposed over stress-strain graph. From these graphs, it could be seen that even the energy rate graphs have followed a similar trend as the cumulative graphs and hit graphs presented above. Again it could be seen that the highest energy rate has been recorded with the specimen having a no defect (Fig. 7b – defect free weld) and the lowest being the one which failed in the heat affected zone (Fig. 7d – HAZ). Moreover, when closely observed, it could be seen that the onset of around 50–75 energy rate is a clear indicator of change of linearity in the stress-strain curve and is also an effective indicator of impending failure.

4.4. Count rate

Figure 8 represents AE count rate *vs* strain interposed over stress-strain graph. From these graphs, it could be observed that even the count rate graphs have followed a similar trend as the cumulative graphs and hit graphs presented above. Again it could be seen that the highest count rate has been recorded with the specimen having a no defect (Fig. 8b – defect free weld) and

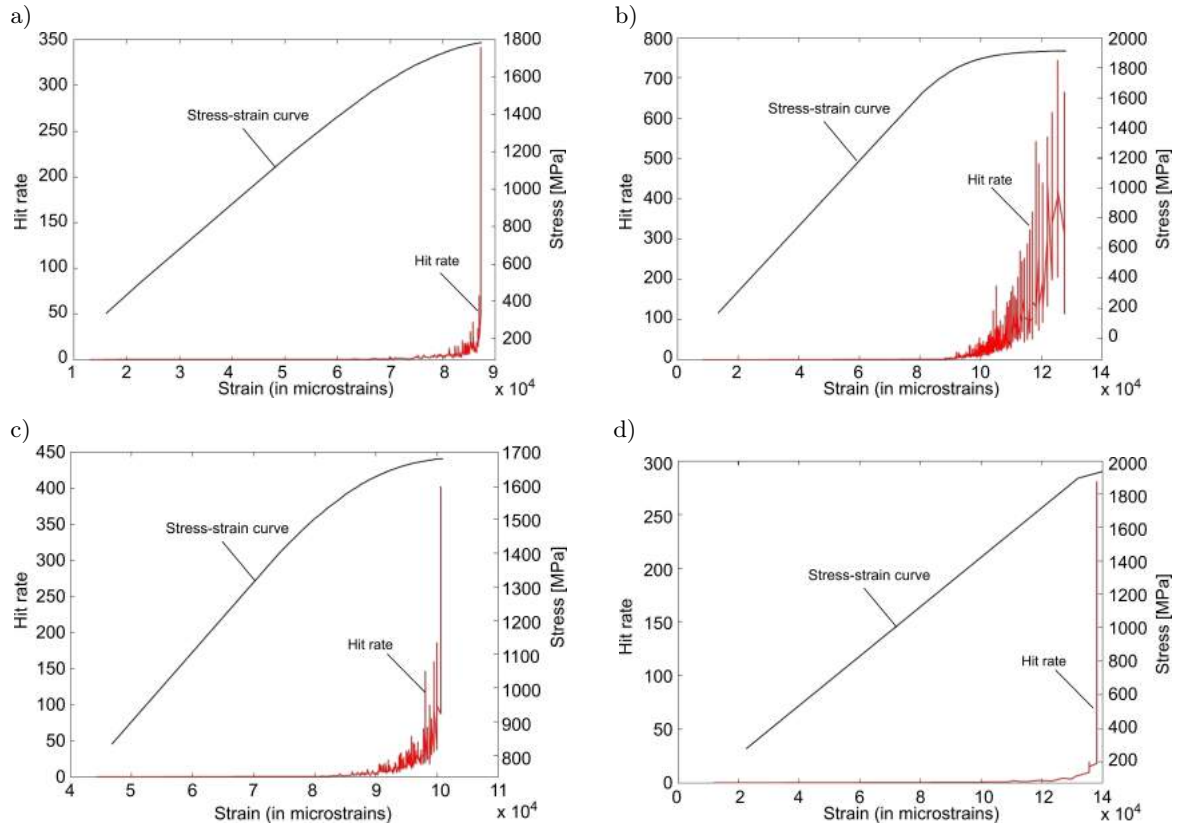

Fig. 6. AE hit rate and stress-strain comparative plot: a) with inherent micro defects, b) with defect free weld, c) with weld defect, d) with HAZ failure.

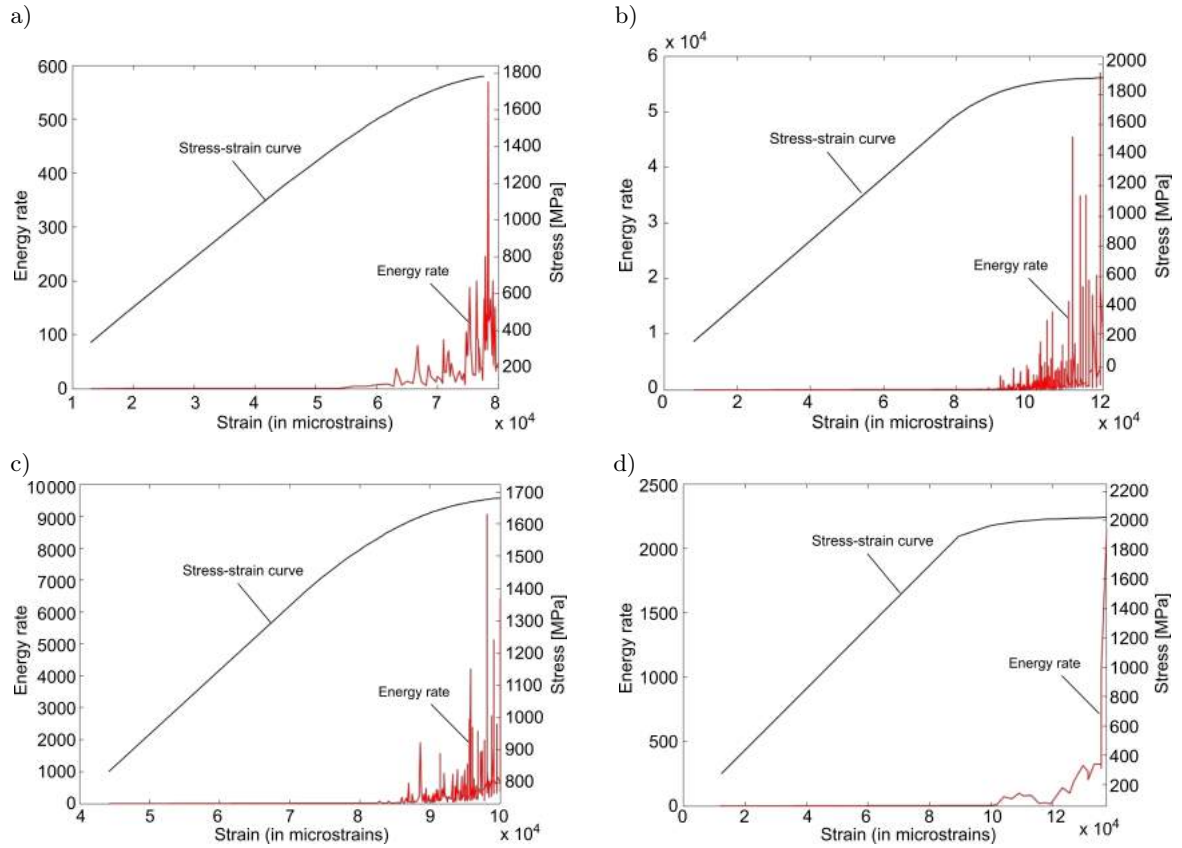

Fig. 7. AE energy rate and stress-strain comparative plot: a) with inherent micro defects, b) with defect free weld, c) with weld defect, d) with HAZ failure.

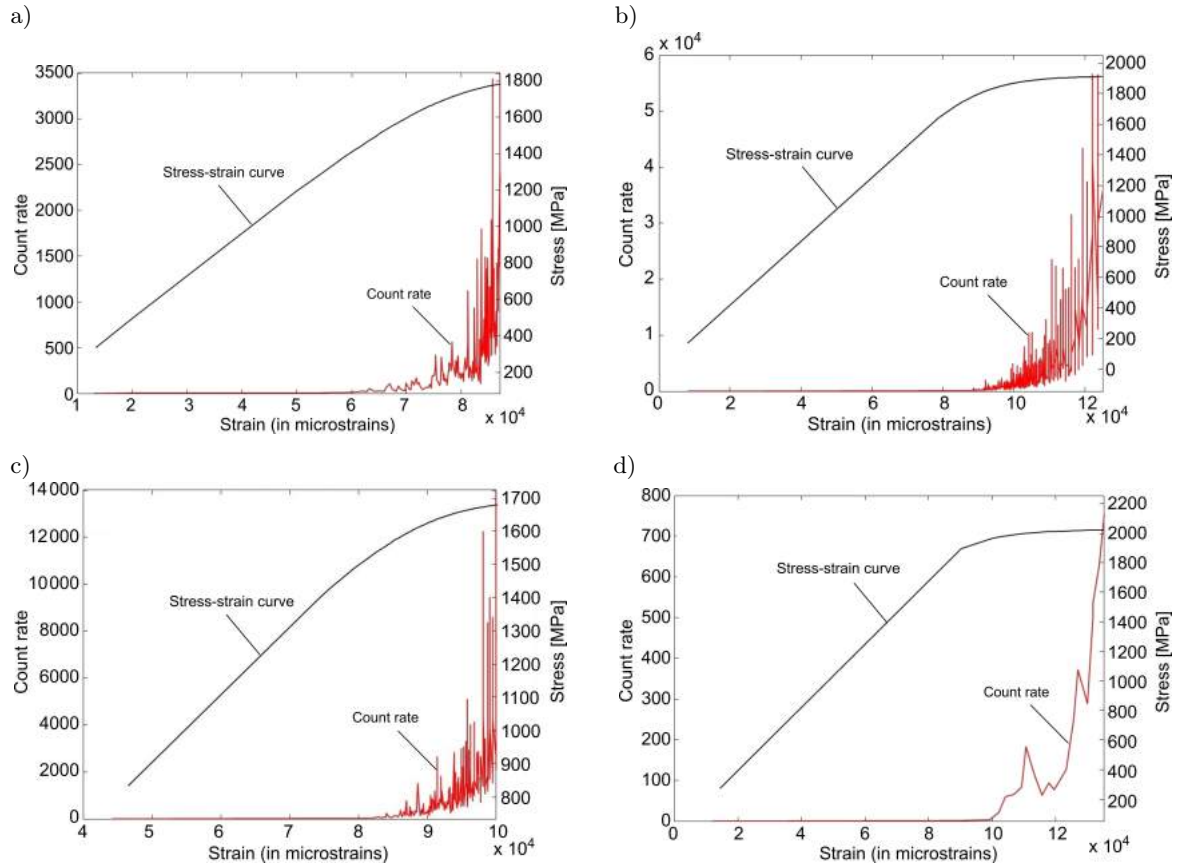

Fig. 8. AE count rate and stress-strain comparative plot: a) with inherent micro defects, b) with defect free weld, c) with weld defect, d) with HAZ failure.

the lowest being the one which failed in the heat affected zone (Fig. 8d – HAZ). Moreover, when critically observed, it could be seen that the onset of around 90–120 counts per second is a clear indicator of change of linearity in the stress-strain curve and is also an effective indicator of impending failure.

4.5. AE amplitude history

Figure 9 represents AE amplitude *vs* strain interposed over stress-strain graph. The AE amplitude distribution data has very vital information about the behaviour of the specimen. Hence, it becomes the most influential parameter in predicting the failure loads of specimens. This distribution data contains all information like defect growth, micro-structural changes, grip noises etc. It could be seen that the initial phases of loading are characterized by relatively lower amplitude signals and as the load increases, there is an increase in the number of high amplitude hits. It could also be observed that the specimen that failed in HAZ (Fig. 9d) had created minimum emissions and the one that was defect free (Fig. 9b) had created maximum emissions. As indicated earlier, it could be seen that more emissions have started close to the onset of yielding/plastic deformation of the material.

4.6. AE counts history

Figure 10 represents AE counts *vs* strain interposed over stress-strain graph. Similar to AE amplitude distribution data, count distribution data also have very vital information about the behaviour of the specimen. But it could not be effectively used in predicting the failure loads because there could also be many low count hits arising out of grip noises. Count-stress correlation helps in the qualitative examination of the structure under test. It could be revealed from all graphs that maximum values for counts are reached at the verge of failure. Hence, until around 95% of the failure load, the maximum counts are around 500 only.

4.7. Amplitude-counts correlation plots

Figure 11 represents two sets of plots each. The first one representing AE amplitude *vs* strain interposed over stress-strain graph and the second one representing AE counts vs strain interposed over stress-strain graph. For a better understanding of the amplitude and count distributions one should look at critical amplitudes and counts in combination. Either a very high amplitude with negligible counts or a very low amplitude with very high counts (a rare

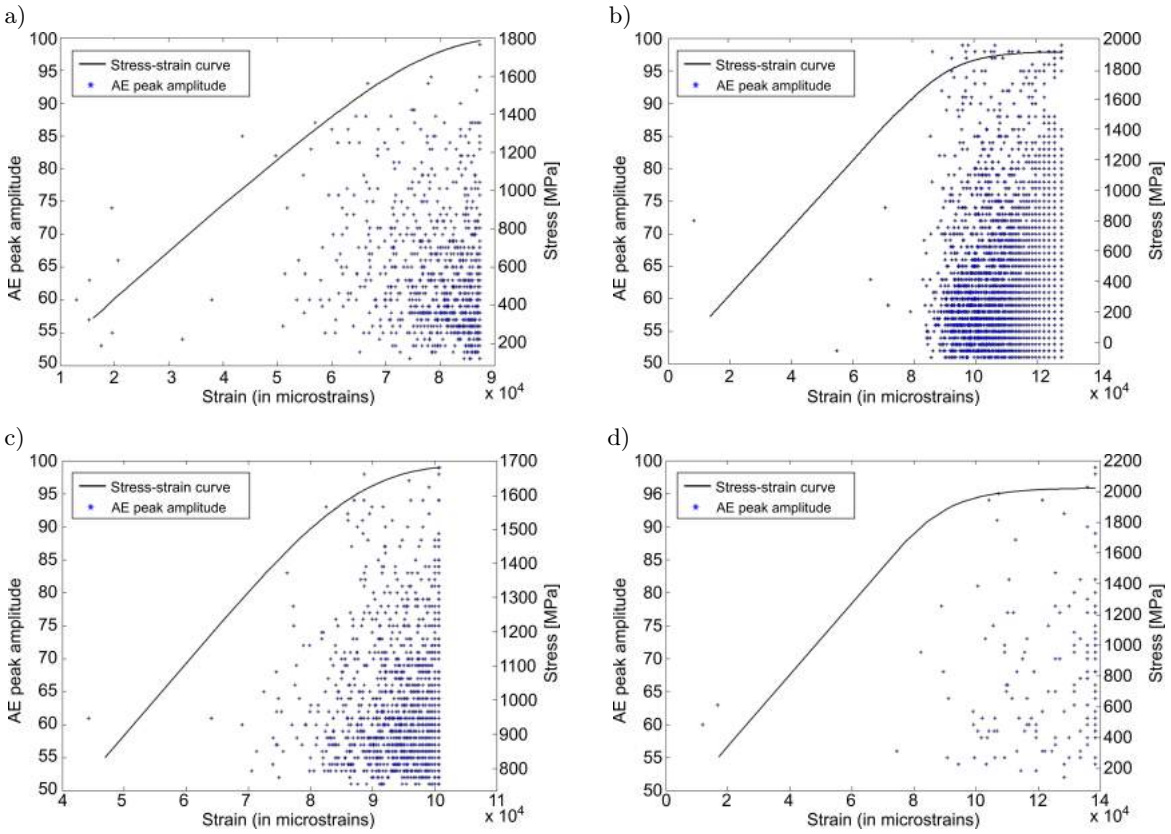

Fig. 9. AE amplitude history and stress-strain comparative plot: a) with inherent micro defects, b) with defect free weld, c) with weld defect, d) with HAZ failure.

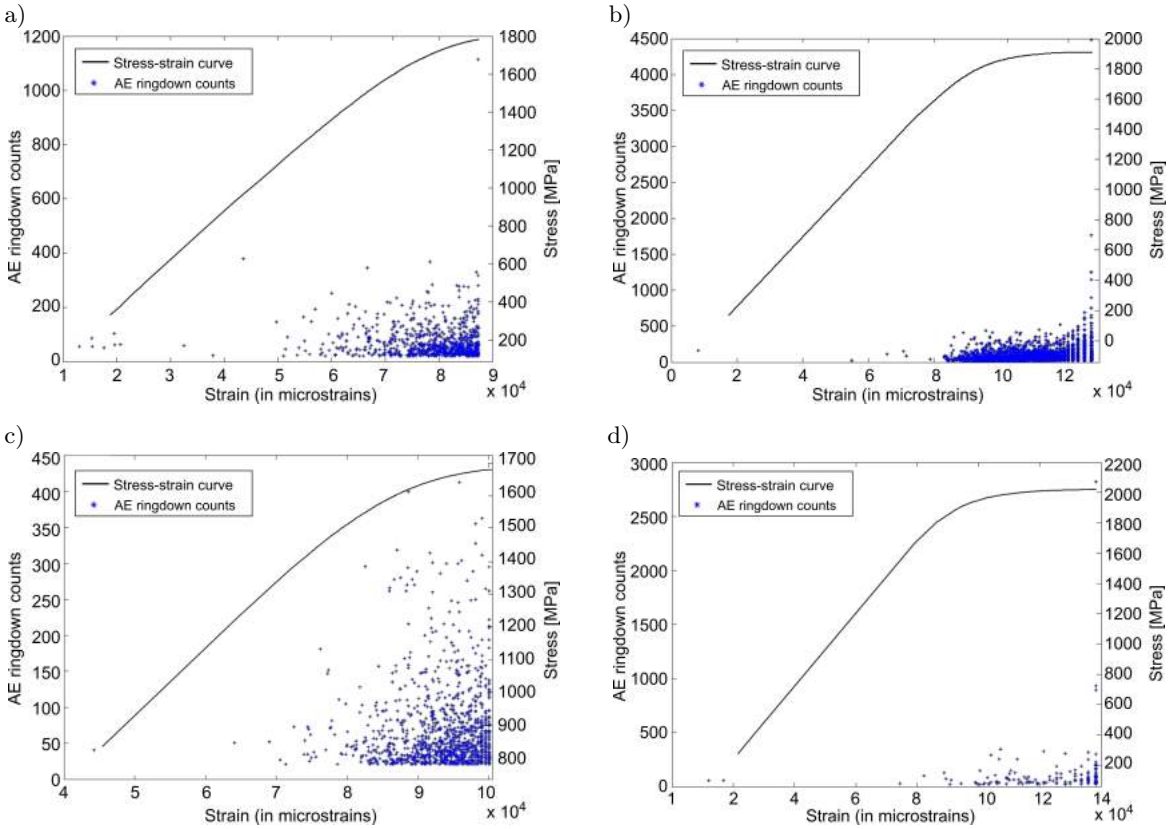

Fig. 10. AE count history and stress-strain comparative plot: a) with inherent micro defects, b) with defect free weld, c) with weld defect, d) with HAZ failure.

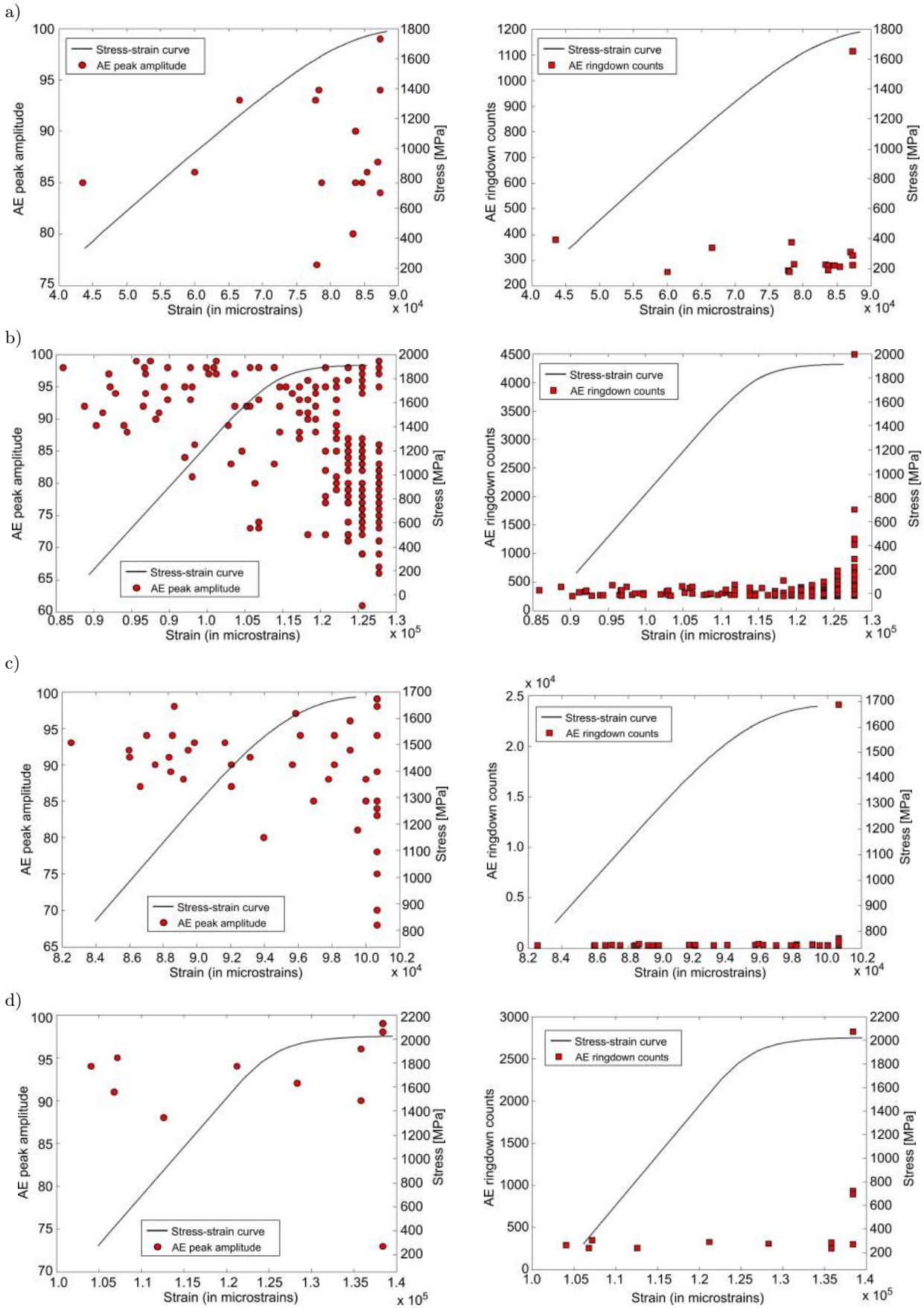

Fig. 11. Filtered AE Data and Stress-Strain comparative plot: a) with inherent micro defects, b) with defect free weld, c) with weld defect, d) with HAZ failure.

case that happens during leaks) generally do not have a significant say on the material failure process (Yamamoti *et al.*, 1980). Hence, it is always better to simultaneously filter both amplitude and counts together. This is even possible while doing online monitoring of rocket motor casings. Based on previous experience and other reported works (Chelladurai *et al.*, 1996), filter amplitude >60 dB and count >250 are considered. The resulting plots are presented in Fig. 11. It could be clearly concluded that the number of occurrences of high amplitude or high count hits keeps increasing with the increasing load. The maximum number of such critical hits (i.e. with amplitude >60 dB and count >250) has happened with the defect free (Fig. 11b) specimen and the HAZ failed specimen (Fig. 11d) scored minimum. Hence, it could be said that the weld failure of the defect free specimen was a highly brittle process and the failure of the specimen in HAZ was a relatively softer one. For such soft failures, the emissions are also quite low.

4.8. Hit-amplitude distribution graphs

There is a direct relationship between the loading of the specimen and the magnitudes of the AE parameters. Of the many parameters used to model AE activity, the distribution of the hit amplitudes is one of the most informative. The amplitude of a given signal provides means to qualitatively determine the forthcoming failure (Pollock, 1981). Therefore, by monitoring the distribution of the amplitudes for many signals during a particular test, insight into the overall damage state of the test specimen may be attained. The mode or maximum peak value of the amplitude distribution can be related to the stress state of the specimen. The Mode shift towards higher amplitudes that is an indicative of increase in higher stress failure mechanisms and a more evenly distributed stress state in the specimen or a higher quality part. Conversely, for other specimens, increased acoustic activities in the vicinity of stress concentration points at lower stresses shift the mode towards lower amplitudes.

The actual hit-amplitude distributions are given in Fig. 12. From these figures, it could be seen that the specimen that failed at a higher stress level (i.e. HAZ failed specimen – Fig. 12d) had a peak shift towards 60 dB and the specimen that failed at a lower stress level (i.e. Specimen with weld defect – Fig. 12c) had a peak shift towards 55 dB.

Acoustic emission signal analysis quantifies flaw growth activity in a structure as it is loaded through descriptive signal parameters such as amplitude, energy, and duration. For example, low amplitude and energy signals are typically associated with microstructural changes while higher amplitude and energy signals typify crack/defect tip movement. The sig-

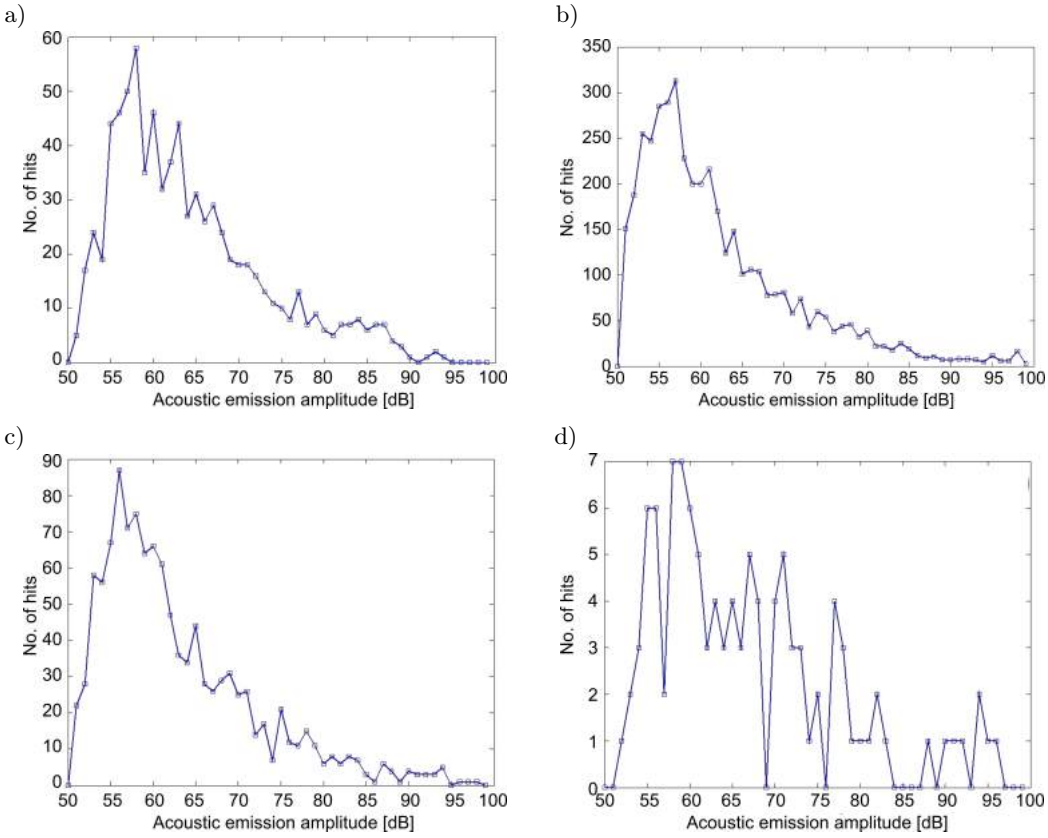

Fig. 12. Actual amplitude distribution plots: a) with inherent micro defects, b) with defect free weld, c) with weld defect, d) with HAZ failure.

nal parameters therefore, provide a reliable measure of the active failure mechanism present during loading (Witos, 2019). The various failure mechanism percentages as recorded by the AE signal distributions have been shown to persist throughout loading (Miller *et al.*, 2005). Acoustic emission amplitude distributions (events/hits *vs* amplitude histogram) have been shown to contain information that allows the identification of failure mechanisms in materials (Pollock, 1981). The various failure mechanisms are typically noticed and are grouped together as characteristic humps or bands in the amplitude distribution. The amplitude bands for such mechanisms viz. plastic deformation and crack growth are widely separated. There are other mechanisms whose characteristic amplitude bands overlap. This overlap in the AE failure mechanism amplitude bands is accentuated by attenuation effects, especially dispersion but in the current study, as the sample size is small, the attenuation effects in the AE waveforms are expected to be minimal.

5. Conclusion

Assessment of structural integrity of pressure vessel casings appropriately or accurately is a major concern for a long time despite various approaches developed. A viable solution is still evading the researchers. Some attempts have been made in studying the AE behaviour of welded samples during tensile deformation. An in-depth understanding of the AE signatures shall pave the way for effective structural integrity evaluation of pressure vessel casings. Maraging steel weldment tensile specimens were subjected to monotonically increasing load unto failure simulating the conditions that are prevalent during proof pressure testing of casings along with continuous AE monitoring to diagnose the damage initiation and growth. These AE signals were processed and analysed. Sixteen welded tensile specimens were tested in the current study. These specimens, due to their inherent micro-structures and defects have failed at varied load levels. The lowest failure load being 70.5 kN and the highest being 84.8 kN. Various failure mechanisms that may lead to penultimate fracture have been examined. The behaviour of weld defect propagation, micro-defect coalescence, heat affected zone (HAZ) rupture have been correlated to AE mechanisms.

The following are the salient observations of the study:

1) A rapid change in the slope of the cumulative activity graph is a vivid indicator of onset of failure.
2) AE hit rate of around 2 hits per second, AE energy rate of around 50–75 energy rate, AE Count rate around 90–120 counts per second, are significant indicator of change of linearity in the stress-strain curve which is the distinct indication of impending failure.
3) Increase in AE amplitude history is an indication of the impending failure or yielding.
4) AE count history is limited to 500 counts at failure.
5) From amplitude-counts correlation plots, it could be said that the weld failure of the defect free specimen was a highly brittle process and the failure of the specimen in HAZ was a relatively softer one. In such soft failures, it is observed that the emissions are also quite low.
6) From hit amplitude correlation graphs, it is qualitatively represented the failure mode.

Most of the AE signatures are correlated to identify the underlying failure of tensile specimens. These indicators can be used for online structural testing of pressure vessels like rocket motor casings and on-set of any of the above, indicates impending failure. It may also be noted that several mechanisms may be impending in causing failure. The appropriate mechanism and the corresponding AE signatures are to be properly applied with. It further necessitates for improved studies with respect to each of these mechanisms and to evolve a stronger failure criteria.

Acknowledgements

This research work is supported by RCI under contract No. DRDO(11)/2018-19/604/Mech.Engg.

References

1. Akbari M., Ahmadi M. (2010), The application of acoustic emission technique to plastic deformation of low carbon steel, *Physics Procedia*, **3**(1): 795–801, https://doi.org/10.1016/j.phpro.2010.01.102.
2. Bohlen J., Chmeliček F., Dobroň P., Letzig D., Lukáč P., Kainer K.U. (2004), Acoustic emission during tensile testing of magnesium AZ alloys, *Journal of Alloys and Compounds*, **378**(1–2): 214–219, https://doi.org/10.1016/jallcom.2003.10.101.
3. Chelladurai T. *et al.* (1999), Acoustic emission response from EB welds of titanium alloy pressure bottles, ISNT, Journal of Nondestructive Testing & Evaluation, www.ndt.net, **19**(3): 34–38.
4. Chelladurai T., Krishnamurthy R., Ramesh Narayanan P., Acharya A.R. (1996), Micro structure studies on M250 maraging steel weldment in relation to acoustic emission, *Trends in NDE Science & Technology. Proceedings of the 14th World Conference on Non-Destructive Testing*, New Delhi, December 8–13, 1996, Vol. 4, pp. 2399–2403.
5. Chelladurai T., Sankaranarayanan A.S., Acharya A.R., Krishnamurthy R. (1995), Acoustic emission response of 18% Ni Maraging steel weldment with inserted cracks of varying depth to thickness ratio, *Materials Evaluation*, **53**(6).

6. Chelladurai T., Sankaranarayanan A.S., Subba Rao S.V., Sarma A.V.S.S.SR., Acharya A.R., Krishnamurthy R. (1996), Acoustic emission technique – an effective tool for the integrity evaluation of M250 Maraging steel aerospace pressure chambers, *Trends in NDE Science & Technology. Proceedings of the 14th World Conference on Non-Destructive Testing*, New Delhi, December 8–13, 1996, Vol. 4, pp. 2409–2412.
7. Cross N.O., Loushin L., Thompson J. (1972), Acoustic emission testing of pressure vessels for petroleum refineries and chemical plants, [in:] *STP505-EB Acoustic Emission*, R. Liptai, D. Harris, C. Tatro [Eds], pp. 270–296, ASTM International, West Conshohocken, PA, doi: 10.1520/STP35393S.
8. Wuriti G.S., Thomas T., Chattopadhyaya S. (2019), Prediction of tensile failure load for maraging steel weldment by acoustic emission technique, [in:] *Advances in Manufacturing Engineering and Materials. Lecture Notes in Mechanical Engineering*, Hloch S., Klichová D., Krolczyk G., Chattopadhyaya S., Ruppenthalová L. [Eds], Springer, doi: 10.1007/978-3-319-99353-9_46.
9. Hay D.R., Chan R.W.Y., Sharp D., Siddiqui K.J. (1984), Classification of acoustic emission signals from deformation mechanisms in aluminum alloys, *Journal of Acoustic Emission*, **3**(3): 118–129.
10. Hill E.V.K. (1992), Predicting burst pressures in filament-wound composite pressure vessels by using acoustic emission data, *Materials Evaluation*, **50**(12): 1439–1445, bibcode: 1992MatEv..50.1439H.
11. Hsu N.N., Hardy S.C. (1978), Experiments in acoustic emission waveform analysis for characterization of acoustic emission sources, sensors and structures, [in:] *Proceedings of the ASME Conference on Elastic Waves and Non-Destructive Testing of Materials*, pp. 85–106.
12. Hwang W., Bae S., Kim J., Kang S., Kwag N., Lee B. (2015), Acoustic emission characteristics of stress corrosion cracks in a type 304 stainless steel tube, *Nuclear Engineering and Technology*, **47**(4): 454–460, doi.org/10.1016/j.net.2015.04.001.
13. Yu J., Ziehl P., Zárate B., Caicedo J. (2011), Prediction of fatigue crack growth in steel bridge components using acoustic emission, *Journal of Constructional Steel Research*, **67**(8): 1254–1260, doi: 10.1016/j.jcsr.2011.03.005
14. Miller R.K., Hill E.V.K., Moore P.O. (2005), *Nondestructive Testing Handbook. Vol. 6: Acoustic emission Testing*, 3rd. ed., American Society for Nondestructive Testing.
15. Pollock A.A. (1981), Acoustic emission amplitude distributions, [in:] *International Advances in Nondestructive Testing. Vol. 7*, McGonnagle W.J. [Ed.], pp. 215–239, Gordon and Breach Science Publishers, New York, NY.
16. Skalskyi V., Andreikiv O., Dolinska I. (2018) Assessment of subcritical crack growth in hydrogen-containing environment by the parameters of acoustic emission signals, *International Journal of Hydrogen Energy*, **43**(10): 5217–5224, doi: 10.1016/j.ijhydene.2018.01.124.
17. Subba Rao V., Jayaseelan D., Satyanarayana N., Viswanathan K. (1996), Analysis of acoustic emission data obtained during pressure testing of M250 maraging steel rocket motor cases, [in:] *Trends in NDE Science and Technology: Proceeding of the 14th World Conference on Non-Destructive Testing*, New Delhi, December 8–13, 1996, Vol. 4, pp. 2427–2450.
18. Witos F. (2019), Properties of amplitude distributions of acoustic emission signals generated in pressure vessel during testing, *Archives of Acoustics*, **44**(3): 493–503, doi: 10.24425/aoa.2019.129264.
19. Yamamoti S., Tsupikawa T., Nakaro M., Veyana H. (1980), Acoustic emission testing of pressure vessels made of 2¼ Cr – 1 Mo steel, [in:] *Non-Destructive Examination in Relation to Structural Integrity*, pp. 19–39.